Neuron, Vol. 33, 75–85, January 3, 2002, Copyright ©2002 by Cell Press

Molecular Rearrangements of the Extracellular Vestibule in NMDAR Channels during Gating

Alexander I. Sobolevsky,[1,3] Christine Beck,[2] and Lonnie P. Wollmuth[1]
[1] Department of Neurobiology and Behavior
State University of New York at Stony Brook
Stony Brook, New York 11794
[2] Abteilung Molekulare Neurobiologie
Max-Planck-Institut für Medizinische Forschung
Jahnstrasse 29
D-69120 Heidelberg
Germany

Summary

Many N-methyl-D-aspartate receptor (NMDAR) channel blockers that have therapeutic potential can be trapped in the closed state. Using a combination of the substituted cysteine accessibility method and open channel blockers, we found that the M3 segment forms the core of the extracellular vestibule, including a deep site for trapping blockers. The M3 segment, as well as more superficial parts of the extracellular vestibule, undergo extensive remodeling during channel closure, but do not define the activation gate, which is located deeper in the pore. Rather, the pore walls lining the extracellular vestibule constrict during channel closure. This movement is essential for coupling ligand binding to activation gate opening and accounts for the different mechanisms of open channel block, including trapping.

Introduction

The N-methyl-D-aspartate receptor (NMDAR), a representative of the family of ionotropic glutamate receptors (GluRs), is critical to neuronal development and synaptic plasticity and has been implicated in acute and chronic cell death, including that associated with a variety of neurological disorders (Dingledine et al., 1999). In the absence of glutamate, the ion channel associated with NMDAR is in the closed or nonconducting state. Agonist binding ultimately leads to a conformational change in the protein that converts the ion channel to the open or conducting state and in some instances to the desensitized state. The ligand binding domain of GluRs, including its crystal structure (Armstrong et al., 1998), as well as determinants of NMDAR desensitization (Krupp et al., 1998; Villarroel et al., 1998), have been characterized. However, the location and molecular composition of the activation gate—the structure that occludes ion fluxes in the closed state—and structures that transfer agonist binding to activation gate movement remain unknown. Defining these issues is critical because the therapeutic potential of many NMDAR channel blockers is related to gating (Parsons et al., 1998).

The channel associated with the NMDAR, like all other ion channels, consists of a water-filled pore divided into intracellular and extracellular vestibules by a narrow constriction. Residues forming these pore domains have been identified (Kuner et al., 1996; Beck et al., 1999). Based on the substituted cysteine accessibility method (SCAM), the channel's narrow constriction and the functionally important N site asparagines are located around the tip of the M2 loop, which also lines the intracellular vestibule (Figure 1). The extracellular vestibule, as contributed by the NR1 subunit, is formed by residues on the N-terminal side of the M1 segment (preM1), the C-terminal part of the M3 segment, and the N-terminal part of the M4 segment.

The extracellular vestibule of NMDAR channels is a target of numerous open channel blockers. One such class of blockers, the so-called "trapping" blockers, includes compounds having clinical significance, such as MK-801, ketamine, phencyclidine, aminoadamantanes, and A-7, as well as small tetraalkylammonium compounds and Mg^{2+} (Huettner and Bean, 1988; MacDonald et al., 1991; Blanpied et al., 1997; Chen and Lipton, 1997; Sobolevsky et al., 1999; Sobolevsky and Yelshansky, 2000). When applied externally, trapping blockers enter open NMDAR channels and bind to a "blocking site" located deep within the pore. Occupancy of this site, however, does not prevent channel closure, and the blocking molecule becomes "trapped" in the pore in the closed state. The interpretation of such a blocking mechanism is that the blocking site is located deeper in the pore than the activation gate, placing the gate in the outer part of the extracellular vestibule (Antonov et al., 1998; Sobolevsky et al., 1999).

In contrast, experiments using SCAM have suggested that the activation gate in NMDAR channels is located deep in the pore, at the level of the N sites or deeper (Beck et al., 1999). Indeed, all of the substituted cysteines in the extracellular vestibule that were accessible in the presence of glutamate, with a single exception, were also accessible in the absence of glutamate. Still, while these results argue against an extracellular location for the gate, their interpretation is not unambiguous given that they are based on the use of high concentrations of the membrane-permeable 2-aminoethyl MTS (MTSEA).

To address this paradox in terms of the location of the gate, we used SCAM in combination with channel blockers to study the functional architecture of the NMDAR channel's extracellular vestibule. We find that the voltage drop and binding of blockers occurs mostly in the deep part of M3, near the narrow constriction, while preM1 and M4 contribute to more external or shallower parts of the vestibule. However, all three domains are involved in gating-related movements but do not constitute the activation gate. Rather, the pore walls in the extracellular vestibule constrict during channel closure, and it is the associated narrowing of the water-filled pore that underlies trapping block.

Results

For our experiments, we coexpressed the NR1 and NR2C subunits since NR1-NR2C channels show no ap-

[3] Correspondence: asobolevsky@notes2.cc.sunysb.edu

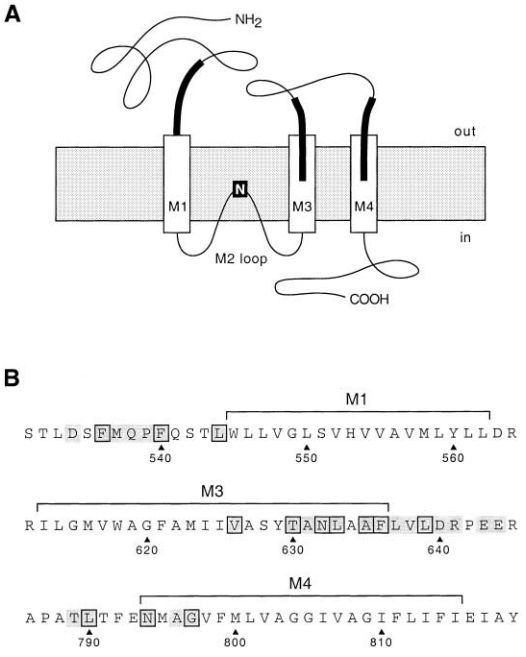

Figure 1. Topology of a NMDAR Subunit

(A) Presumed membrane topology of the NMDAR subunits (NR1 and NR2). Hydrophobic segments M1, M3, and M4 are shown as white boxes. The thick lines indicate regions proposed to form the extracellular vestibule as contributed by NR1 (Beck et al., 1999). The N site asparagine (shown in a closed box) (position 598 in NR1 and 593 in NR2C) and the channel's narrow constriction are positioned at the tip of the M2 loop.

(B) Amino acid residues of the NR1 subunit within and around the M1, M3, and M4 segments. Positions accessible to reaction with MTS reagents are highlighted in gray. In the present study, we explored a subset of these exposed cysteines (boxes). The numbering is for the mature protein.

parent desensitization (Krupp et al., 1996) and will therefore exist either in the closed state (absence of glutamate) or both in the closed and open states (presence of glutamate). Figure 1 shows the domains proposed to contribute to the extracellular vestibule (thick lines in Figure 1A) as well as corresponding exposed positions (highlighted in gray in Figure 1B) for the NR1 subunit (Beck et al., 1999). We studied in detail only a subset (boxes) of these exposed positions, initially selecting those that encompass domains, and then, in the case of M3, selecting nearly all because of its central role in forming the extracellular vestibule.

Modification Rate of Cysteine-Substituted NMDAR Channels in the Presence of Glutamate

Figure 2A shows glutamate-activated currents recorded in *Xenopus* oocytes expressing cysteine-substituted NMDAR channels. The application of MTS reagents (thick line) typically reduced current amplitudes (e.g., F536C, T630C, and N794C in Figure 2A), but in two instances, N598C (Figure 2A) and A635C, it increased them. In most cases, modification was completely irreversible. For certain mutant channels, we observed a reversible component that was faster and smaller in magnitude (<20%) than the irreversible component. We assumed that the irreversible component reflected chemical modification of substituted cysteines. For the N sites (N593C in NR2C and N598C in NR1), we used MTSET as the reagent because of the complex modification kinetics of these channels by MTSEA (see Kuner et al., 1996). For all other mutant channels, we used MTSEA since it produced a much stronger effect on current amplitudes than MTSET.

For all cysteine-substituted channels, changes in current amplitudes with the MTS application were well fitted by a single exponential function. We used the time constant derived from these fits to estimate the apparent second-order rate constant for chemical modification in the presence of glutamate, k (Equation 2). Mean k values are shown in Figure 2B. Consistent with previous results (Beck et al., 1999), the rate constant for modification by MTSEA in glutamate varied greatly from about 65 $M^{-1}s^{-1}$ for L544C to 1.2 $\times$ 10^5 $M^{-1}s^{-1}$ for N794C. Such variations in the rate of reactivity for charged MTS reagents may reflect differences in (1) the local electrostatic potential, (2) the degree of sulfhydryl group ionization of the substituted cysteine, and/or (3) the steric availability of the sulfhydryl group on the protein surface (Karlin and Akabas, 1998).

Modification rates of the N sites by MTSET were very slow. The k value for N598C, 57 $M^{-1}s^{-1}$, was the slowest when MTS reagents were applied in the presence of glutamate. In part this may reflect the larger size of MTSET compared to MTSEA especially since the N sites are positioned at or near the channel's narrow constriction (Wollmuth et al., 1996).

Voltage Drop in the Extracellular Vestibule Occurs Mainly within the M3 Segment

The N site asparagines are presumably positioned deep in the pore, but the relative positioning of extracellular vestibule elements is unknown. To address this issue, we measured the rate of reaction of MTS reagents with exposed cysteines in the presence of glutamate at different membrane voltages (Figure 3). Figure 3A illustrates such recordings for the MTSEA-induced inhibition and potentiation of currents for V626C and A635C, respectively. For V626C, the modification rate became faster with membrane hyperpolarization, whereas for A635C it was independent of membrane voltage (Figure 3B). A fit of the rate constant, expressed in a logarithmic form ($-$ (RT/F) ^{x}Lnk), with Equation 4 gives an estimation of the fraction of the transmembrane electric field, $z\delta$, that the MTS reagent passes to reach the exposed cysteine. The $z\delta$ values for all cysteine-substituted channels tested are summarized in Figure 3C. The strongest voltage dependence with $z\delta$ around 0.6–0.7 was observed for the N sites and the two deepest positions in M3, V626, and T630. Positions N632 and L633 in M3, and L544 in preM1 showed progressively weaker voltage dependence. The reaction rates for all other positions were voltage independent.

The $z\delta$ values are an estimate of the transmembrane electric field and do not necessarily correspond to any physical distance. Their absolute magnitude can also be influenced by remote electrostatic and structural factors. We therefore measured the voltage dependence of the rate of reactivity of the neutral MTS reagent MMTS

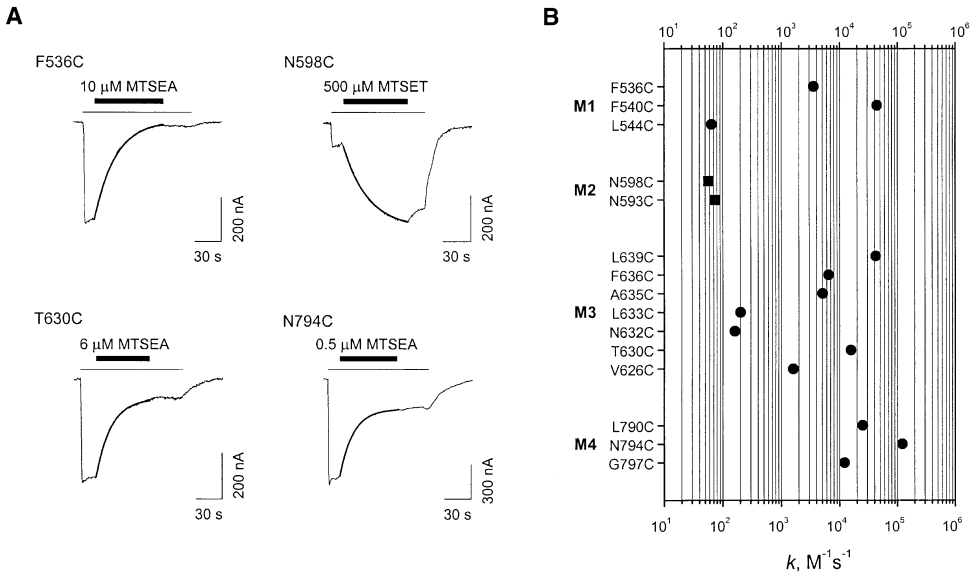

Figure 2. Modification Rate of Exposed Cysteines in the Presence of Glutamate

(A) Whole-cell currents recorded from *Xenopus* oocytes expressing NR1(F536C)-NR2C, NR1(N598C)-NR2C, NR1(T630C)-NR2C, or NR1(N794C)-NR2C. Currents were elicited by a 120 s application of glutamate (thin lines) at a holding potential (V_h) of −60 mV. MTS reagents (thick lines) were applied continuously for ~80 s. Changes in current amplitudes during the MTS application are fitted by a single exponential function (thicker line in current plot) with time constants of 23.7 s for F536C, 26.8 s for N598C, 17.3 s for T630C, and 15.0 s for N794C.

(B) Apparent second-order rate constants, k, for chemical modification of substituted cysteines in the presence of glutamate. These constants were derived using Equation 2 and are shown as circles for MTSEA and squares for MTSET. SEM values are smaller than the symbol size ($n > 3$). All of the cysteine-substitutions, except for N593C, were present in NR1, which was coexpressed with wild-type NR2C. NR2C(N593C) was coexpressed with wild-type NR1.

with V626. These rates were voltage independent ($z\delta = -0.07 \pm 0.03$), suggesting that most of the voltage dependence for MTSEA at this position arises from a direct interaction between the reagent's charge and the transmembrane electric field. This result, along with the consistent overall pattern of voltage dependence, suggests that $z\delta$ represents an approximate index of the relative positioning of exposed residues. Thus, since most of the voltage drop occurs across M3, this segment forms the deep core of the extracellular vestibule with the deepest positions V626 and T630 located near the N sites. L544 in preM1 experiences less of the electric field and accordingly may be located somewhat more superficially. All other domains are positioned even more externally, being located outside the transmembrane electric field.

State-Dependent Changes in the Modification Rate of Exposed Cysteines

In the absence of glutamate, exposed cysteines in the extracellular vestibule are also accessible to MTSEA (Beck et al., 1999), suggesting that they are on the extracellular side of the activation gate. MTSEA is the smallest positively charged MTS reagent and can exist in a nonionized form (see Karlin and Akabas, 1998). Figure 4 shows the accessibility of exposed residues in the extracellular vestibule to the much larger and permanently charged PTrEA, either in the presence (left panel) or absence (right panel) of glutamate. As for MTSEA, all of the positions were accessible in the absence of glutamate, even those presumably positioned deep in the pore, including V626 and T630 in M3. Still, these experiments were carried out using high concentrations of reagents (2 mM) for long periods of time (60 s) and may have missed differences in state-dependent accessibility. We therefore measured the modification rate for cysteine-substituted channels in the absence of glutamate (Figure 5).

Figure 5A illustrates our protocol to measure modification rates in the absence of glutamate. MTS reagents (solid bars) were applied in the presence of the competitive NMDAR antagonist, APV (open boxes). Glutamate-activated current amplitudes, when plotted as a function of the cumulative time of MTS exposure (Figure 5B), give the time course of modification. We used the time constant of the fitted exponential to these plots to define the apparent rate constant for modification in the absence of glutamate, k_{APV} (Equation 2). Figure 5C shows the k_{APV} values (open symbols), in superposition with the k values in the presence of glutamate (closed symbols), with the ratio of these rate constants, k/k_{APV}, summarized in Figure 5D. The k/k_{APV} ratio is underestimated for the N sites (cut bars).

Many positions showed more than a 10-fold difference between reaction rates in the presence and absence of glutamate, including positions located deep in the electric field: N593, N598, V626, and T630. However, a strong state dependency was also observed for F540 and L544 in M1, A635 and L639 in M3, and N794 in M4. Intermixed with these positions in M3 were several positions that showed much less state dependence (e.g., N632 and F636). This reduced state dependency, however, was not due to MTSEA accessing these positions via the lipid phase since a comparable or smaller ratio was found when the permanently charged MTSET was used as the test reagent (squares, Figure 5C).

The slower modification rates in the absence of gluta-

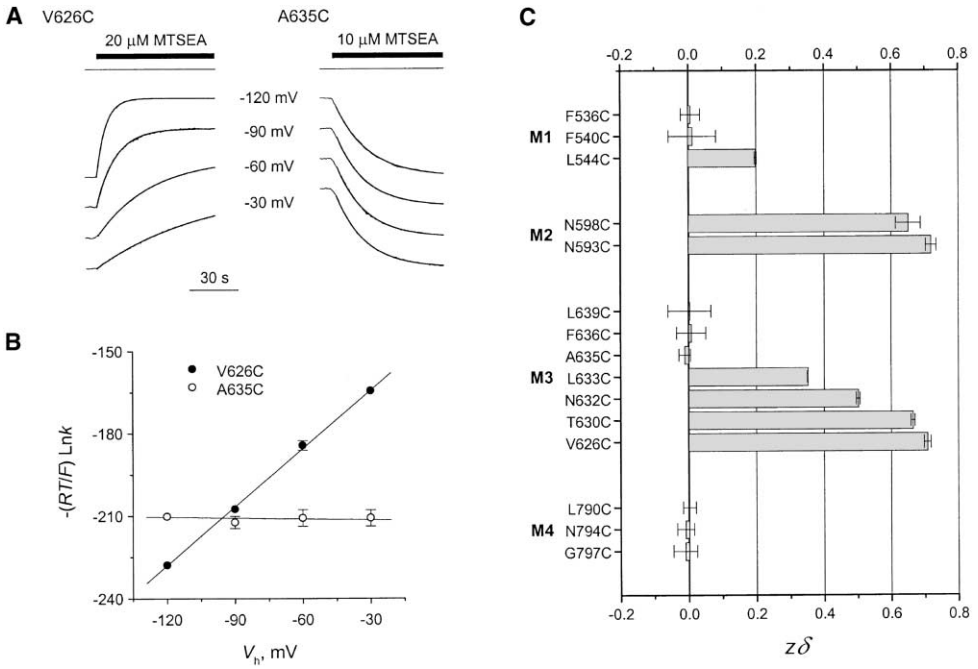

Figure 3. Voltage Dependence of the Modification Rate in the Presence of Glutamate

(A) Current traces show MTSEA-induced inhibition of V626C and potentiation of A635C at different membrane voltages (−120, −90, −60, and −30 mV). The protocol is the same as that in Figure 2A. Currents are normalized and fitted by a single exponential function with time constants, at −120, −90, −60, and −30 mV, of: 5.7 s, 11.8 s, 33.3 s, and 67.9 s for V626C; and 20.3 s, 17.9 s, 17.9 s, and 18.3 s for A635C.

(B) Modification rate as a function of the holding potential, V_h. The straight lines through the points are fits with Equation 4. Their slopes give $z\delta$: 0.71 ± 0.01 for V626C and −0.01 ± 0.02 for A635C.

(C) Mean $z\delta$ estimated using the method described in (B). Recordings were made from 3 to 13 cells at each voltage.

mate for positions within all three pore-forming regions suggest that with channel closure, they become less reactive, which we interpret as meaning they are less accessible. The state-dependent modification rates could reflect that we applied MTS reagents differently (continuous versus pulsive protocols) to derive the rate constants. However, reaction rates in the presence of glutamate using a pulsive protocol, as in Figure 5A but with MTSEA applied during the glutamate application, were indistinguishable from those derived using the continuous protocol in Figure 2A (1420 ± 90 $M^{-1}s^{-1}$ for V626C, 130 ± 10 $M^{-1}s^{-1}$ for N632C, and 35700 ± 400 $M^{-1}s^{-1}$ for L639C using the

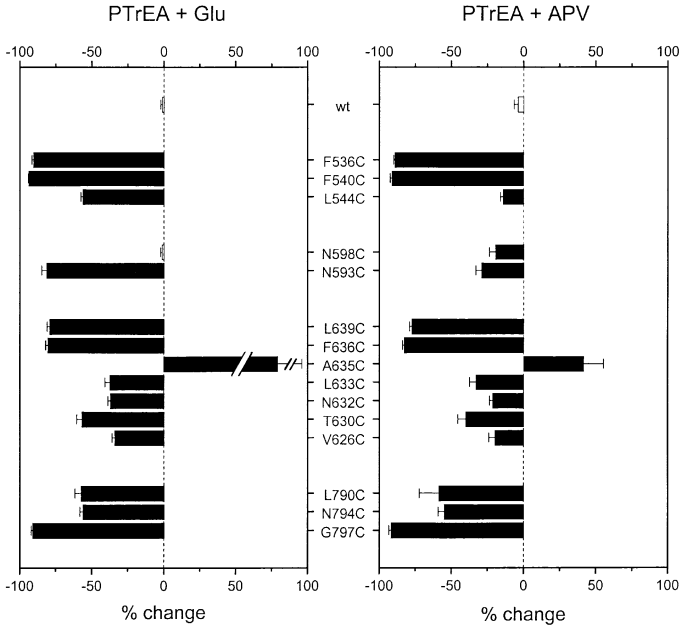

Figure 4. Accessibility of Exposed Cysteines to PTrEA

Mean percent change in current amplitudes measured before (I_{pre}) and after (I_{post}) exposure to PTrEA (2 mM) either in the presence (left panel) or in the absence (right panel) of glutamate. Accessibility was measured using steady-state reactions (see Experimental Procedures). Left and right pointing bars indicate inhibition and potentiation, respectively ($n > 4$). Filled bars indicate a statistical difference between I_{post} and I_{pre}. For N598C in the presence of glutamate, PTrEA produced both a potentiating and an inhibiting effect on current amplitudes, producing no net change in I_{post}. Cut bar for A635C indicates that currents were potentiated by more than 100%.

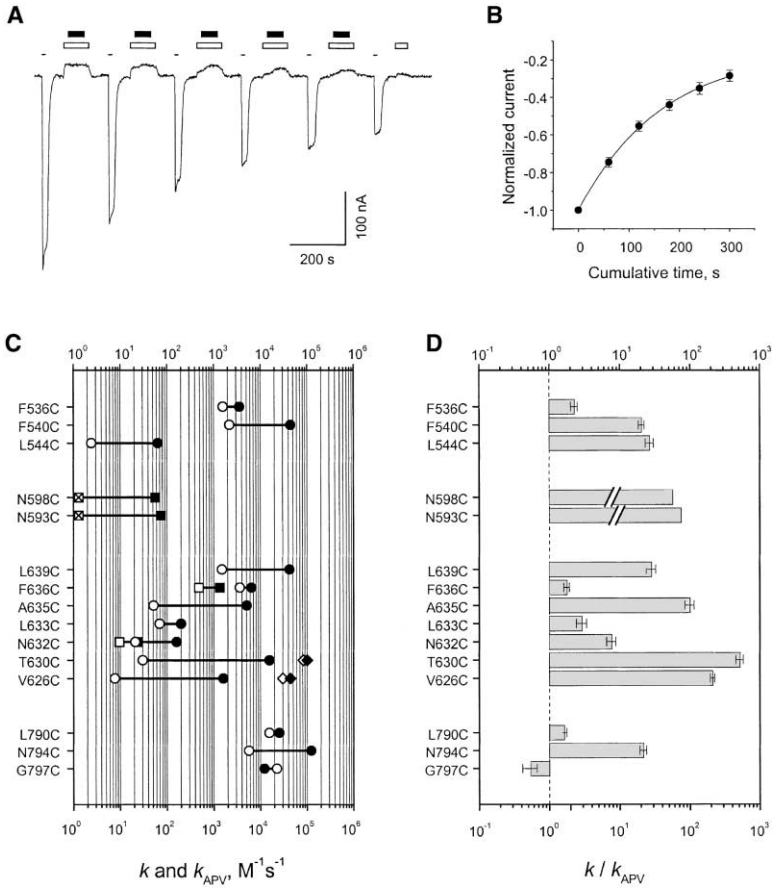

Figure 5. Modification Rate of Exposed Cysteines in the Absence of Glutamate

(A) Pulsive protocol to assay modification rates in the absence of glutamate. The example shows NR1(L639C)-NR2C. V_h was −60 mV. 1 min after a 15 s test glutamate application (thin line), APV (100 μM, open box) was applied for 1.5 min. The MTSEA application (4 μM, closed box, 1 min) was started 15 s after the beginning and finished 15 s before the end of the APV exposure. After APV, the cell was washed for 1.25 min before the next test glutamate application. The application of APV as well as NMDAR channel blockers (Figures 6–7) reduced leak currents in oocytes injected with wild-type and all mutant channels but not in noninjected oocytes. In all instances, this non-glutamate-activated component was ~10% as large as the glutamate-activated component and did not affect the quantification of the rate constants.

(B) Normalized glutamate-activated current amplitudes as a function of cumulative time of exposure. Points represent the average of five cells. Data are fitted by a single exponential function (τ = 166 s).

(C) Second-order rate constants for modification of cysteines in the absence (k_{APV}, open symbols) or in the presence (k from Figure 2B, solid symbols) of glutamate. Rate constants are for MTSEA (circles), MTSET (squares), or Ag^+ (diamonds). Reaction rates for N593C and N598C in the absence of glutamate (crossed squares) could not be determined properly because they required high concentrations of MTSET (>2 mM), which had nonspecific effects on membrane currents. These rates were not faster than 1 $M^{-1}s^{-1}$ but were assigned this value. SEM are smaller than the symbol size (n > 4).

(D) Ratio of the rate constants measured in the presence or absence of glutamate, k/k_{APV}, for MTSET (N593 and N598) and MTSEA (all other positions). Cut bars indicate that k/k_{APV} for N593C and N598C is greater than 74 and 57, respectively.

pulsive protocol compared to 1600 ± 110 $M^{-1}s^{-1}$, 160 ± 20 $M^{-1}s^{-1}$, and 42000 ± 6000 $M^{-1}s^{-1}$, respectively, using the continuous protocol). Further, the degree of current inhibition (I_{post}/I_{pre}) in the absence of glutamate for V626C was not significantly different whether MTSEA (1 mM) was applied using a long 5 min application (0.42 ± 0.06, n = 3) or five 1 min applications with 3 min intervals between them (0.39 ± 0.03, n = 3). Thus, our estimation of the state dependence does not depend on the protocol used to derive the rate constant.

We also used the small sulfhydryl reagent Ag^+ to probe accessibility of several positions located deep in the pore, including V626 and T630 in M3, as well as N594 in the NR2C M2 loop (N594 is adjacent to the N site). For both V626 and T630, the reaction rates for Ag^+ (200 nM) were indistinguishable in the presence and absence of glutamate (diamonds, Figure 5C). In contrast, for N594 (data not shown), a 5 min cumulative exposure to Ag^+ (200 nM) reduced current amplitudes by 53% ± 12% (n = 5) in the presence of glutamate but was without effect in the absence of glutamate (0% ± 3%, n = 4). Such a binary-gated access for N594 and the unimpeded access for V626 and T630 rule out the possibility that the high k/k_{APV} values for MTSEA reactivity with V626 and T630 (210 and 510, respectively) arise because of a nonzero channel open probability in the absence of glutamate, and strongly support the idea that the activation gate is located deeper in the pore than position V626.

Protection of Exposed Cysteines by Trapping Blockers

To understand the mechanism of trapping block in NMDAR channels, we studied whether exposed cysteines in the extracellular vestibule could be protected by such blockers. For these experiments, we used amantadine (AM) since it has relatively fast blocking kinetics (Sobolevsky and Yelshansky, 2000), allowing us to use a pulsive protocol to monitor unmodified channels. In wild-type NR1-NR2C, the IC_{50} for the block by AM at −60 mV was 10.4 ± 0.3 μM (n = 5). All mutant channels showed a comparable affinity except for those containing substitutions of the N sites where the block was attenuated (N593C, 46.9 ± 0.3 μM, n = 3; and N598C, 108 ± 7 μM, n = 4). As shown in Figure 6A, AM (500 μM, open boxes) blocked glutamate-activated currents completely, attenuating, like APV, some portion of the leak current. Termination of the agonist and the blocker coapplication was followed by a transient inward tail current typical of fast open channel blockers (e.g., Sobolevsky et al., 1999). MTS reagents were applied in the presence of AM under which

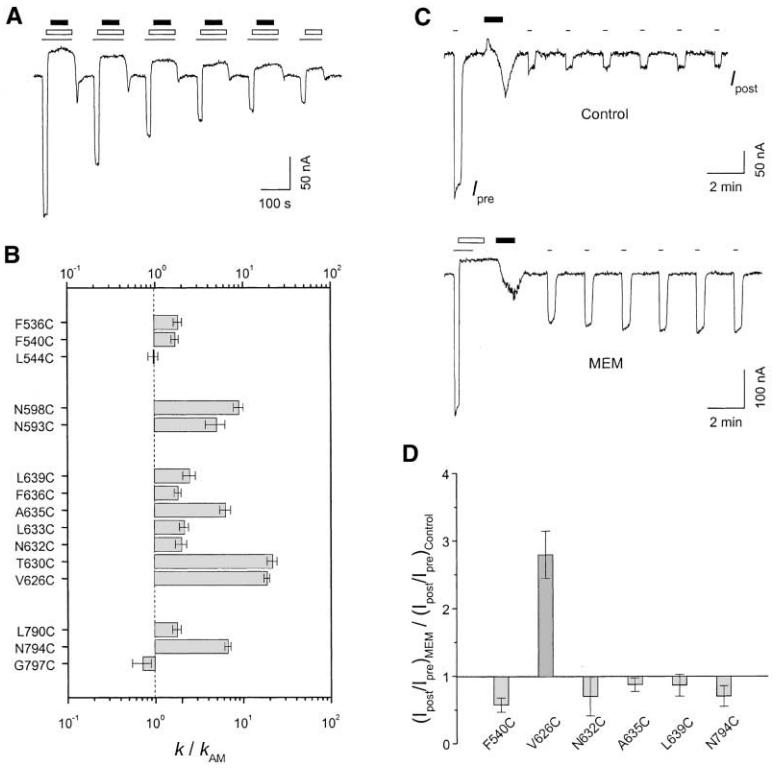

Figure 6. Protection of Exposed Cysteines by Trapping Blockers

(A) Protocol to assay the protection of exposed cysteines by amantadine (AM). The example shows NR1(F540C)-NR2C. After a 15 s test glutamate application (thin line), AM (500 μM, open box), and glutamate were coapplied for 1.5 min. The MTSEA application (0.2 μM, closed box, 1 min) started 15 s after the beginning and finished 15 s before the end of the AM application. After AM, the cell was washed for 1.25 min before the next test glutamate application.

(B) Ratio of the rate constants measured in the absence or presence of AM, k/k_{AM}, all in the presence of glutamate. k_{AM} ($n > 4$) was quantified similar to k_{APV} (Figure 5).

(C) Protocol to assay the protection of exposed cysteines by memantine (MEM) trapped in the channel. The example shows NR1(V626C)-NR2C. Glutamate (thin lines, 15 s) was applied either before (I_{pre}) or after (I_{post}) MTSEA (5 mM, closed box, 1 min). In the test recording (lower trace), glutamate and MEM (200 μM, open box) were coapplied for 45 s, after which MEM was applied alone for 30 s. The cell was then washed for 30 s before the MTSEA application. After MTSEA removal, the cell was washed for 1.25 min before the test glutamate application. At the high concentration of 5 mM, MTSEA induced reversible changes in the baseline current. Similar changes occurred with noninjected oocytes. We also carried out the above experiments applying MTSEA in the continuous presence of APV (as in Figure 5A). The results in the presence and absence of APV were indistinguishable.

(D) Ratio of the change in current amplitudes in MEM, $(I_{post}/I_{pre})_{MEM}$, relative to the control, $(I_{post}/I_{pre})_{Control}$ ($n > 4$). Concentrations of MTSEA were selected to generate 50%–90% of the maximal effects after a 1 min exposure (based on the rates in Figure 5C) and were 10 μM (F540C), 5 mM (V626C), 2 mM (N632C), 500 μM (A635C), 20 μM (L639C), or 10 μM (N794C). Only for V626C was $(I_{post}/I_{pre})_{MEM}$ significantly larger than $(I_{post}/I_{pre})_{Control}$.

conditions we derived the rate constant k_{AM}. Figure 6B shows the ratio k/k_{AM}.

The largest decrease in reactivity occurred for positions V626 and T630, but even for these positions, the protecting effect of AM was relatively small, presumably reflecting the fast unblocking kinetics of AM. A smaller decrease was observed for positions N593 and N598. However, the attenuated block in these channels by AM suggests that the N sites interact with AM and accounts for the reduced protecting action of AM. The action of all trapping blockers, including AM, is strongly voltage dependent (e.g., Huettner and Bean, 1988; Blanpied et al., 1997). Thus, these four positions—the N sites, and V626 and T630 in M3 that show the strongest voltage-dependent reactivity (Figure 3C)—define the deepest site for trapping blockers in NMDAR channels.

Along with these four positions, AM protected other positions as well (Figure 6B), notably A635 in M3 and N794 in M4. A second, voltage-independent blocking site for aminoadamantane derivatives, including AM, exists in open NMDAR channels (Sobolevsky and Koshelev, 1998). Since A635 and N794 show voltage-independent accessibility (Figure 3), they may contribute to this additional blocking site.

Trapping Block Occurs Only Deep in the Pore

The defining feature of trapping blockers is that they are "trapped" in the closed state of the channel. In the presence of glutamate, AM protects positions both deep in the pore, around the N sites, as well as those located more externally. To identify where trapping occurs, we applied MTSEA, in the absence of glutamate, to channels that presumably contained a trapped blocking molecule (Figures 6C and 6D). AM, like other adamantane derivatives, are not perfectly trapped, showing a slow unblocking in the closed state (Blanpied et al., 1997; Sobolevsky et al., 1998). To maximize the number of closed channels still containing a blocker before the MTSEA application, we used memantine (MEM) as the test blocker. MEM is another adamantine derivative that has the same mechanism of block as AM but a much slower unblocking rate (Blanpied et al., 1997; Sobolevsky et al., 1998; Sobolevsky and Yelshansky, 2000). These experiments were carried out for one representative of the four deep positions (V626) as well as more external positions, including those apparently protected by AM in open NMDAR channels.

Figure 6C illustrates the experimental protocol. In the control recording (upper trace), current amplitudes following the MTSEA application in the absence of glutamate were only 10% of those before application. In the test recording (lower trace), MEM (open box) was applied in the presence of glutamate and then glutamate was removed. Many of the channels therefore were closed with MEM trapped in them. Glutamate-induced currents following the MTSEA application were again reduced in amplitude, but the relative degree of reduction was much less. To

compare current reductions in the presence and absence of MEM, we quantified the ratio of the current amplitudes before and after the MTSEA application in the control, $(I_{post}/I_{pre})_{Control}$, and in the test, $(I_{post}/I_{pre})_{MEM}$, conditions (Figure 6D). $(I_{post}/I_{pre})_{MEM}$ was significantly greater than $(I_{post}/I_{pre})_{Control}$ only for position V626, indicating that this position was protected from reaction with MTSEA and strongly supporting the idea that trapping block occurs deep in the extracellular vestibule.

Protection of Exposed Cysteines by 9-Aminoacridine

Sequential or "foot-in-the-door" blockers are another example of open channel blockers (Yeh and Armstrong, 1978). They differ from trapping blockers in that the channel cannot close when occupied by the blocker presumably because of their large size (Antonov et al., 1998; Sobolevsky et al., 1999). We took advantage of one such blocker, 9-aminoacridine (9-AA) (Benveniste and Mayer, 1995; Sobolevsky, 1999), as an additional probe to study the location of blocking sites and the conformational changes associated with channel gating (Figure 7).

Figure 7A illustrates the protocol we used to assay the modification rate in 9-AA. Here, MTS reagents were applied in the presence of 9-AA but in the absence of glutamate. Figure 7B compares the modification rate obtained in 9-AA, $k_{9\text{-}AA}$, to that obtained in glutamate, k. We used k as the reference since channels blocked by 9-AA are presumably locked in the open state. A greater than 10-fold decrease in the modification rate was observed for only four positions, N593, N598, V626, and T630. These same positions are also most strongly protected by AM, indicating that the deep blocking site for trapping blockers and 9-AA coincide. The small protection seen at more external positions (e.g., F536, F540, and N794) could reflect an additional blocking site for 9-AA as suggested previously by the analysis of 9-AA blocking kinetics (Sobolevsky, 1999; see also Costa and Albuquerque, 1994). Additionally, more than a 10-fold increase in $k_{9\text{-}AA}$, as compared to k, occurred for positions L633 and A635 in M3, suggesting that 9-AA increases the exposure of these positions beyond simply locking them in the open state.

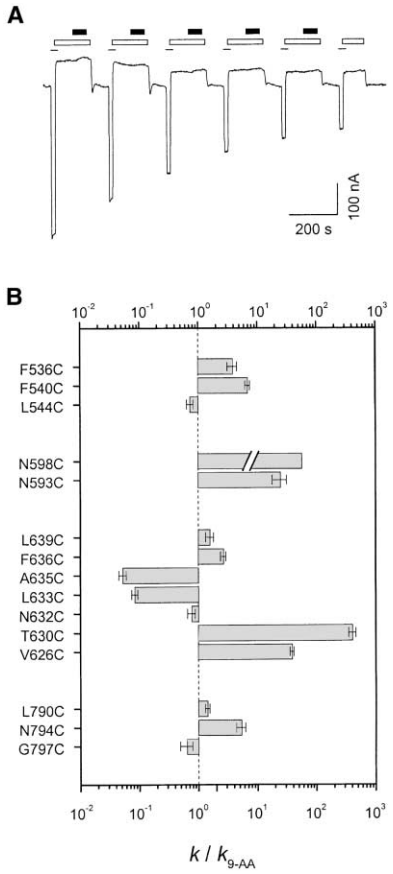

Figure 7. Protection of Exposed Cysteines by 9-Aminoacridine

(A) Pulsive protocol to assay the protection of exposed cysteines by 9-aminoacridine (9-AA). The example shows NR1(F636C)-NR2C. After a 15 s test glutamate application (thin line), glutamate and 9-AA (200 μM, open boxes) were coapplied for 15 s. Glutamate was then removed, and 1 min later, MTSEA (closed box, 1 min) was applied in the continuous presence of 9-AA. After MTSEA removal, the cell was bathed an additional 15 s in 9-AA and then was washed for 1.25 min before the next test glutamate application.

(B) Ratio of the rate constants measured in the presence of glutamate, k, to those in the presence of 9-AA, $k_{9\text{-}AA}$ ($n > 4$). Cut bar indicates that $k/k_{9\text{-}AA}$ for N598C is > 57.

Discussion

The interpretation of our results is limited by the assumptions of the SCAM. Of particular concern is the assumption that the cysteine substitution itself does not alter significantly the structure of the protein. This assumption, while difficult to completely rule out, is supported by the findings that mutant channels were comparable to wild-type in terms of current amplitudes and EC_{50} for glutamate (data not shown) and, except for the N site substitutions, open channel block. We also assume that MTS reagents react predominantly with exposed cysteines via the water interface. As our test reagent, we typically used MTSEA, which can exist in a nonionized form. However, in complimentary experiments, we also used the permanently charged reagents Ag^+, MTSET, and PTrEA, and their outcome was consistent with those using MTSEA.

Location of the Activation Gate in NMDAR Channels

In the closed state, the activation gate occludes the water-filled pore, preventing ion fluxes. Our results indicate that elements forming the extracellular vestibule as contributed by the NR1 subunit remain water accessible in the closed state. Indeed, positions deep in the transmembrane electric field—the N sites (N598 and N593) and V626 and T630 in M3—are accessible in the closed state to the large-sized MTS reagent, PTrEA, with a size-limiting diameter of ~8 Å (Figure 4). Further, the access of Ag^+, which has a size comparable to that of Na^+, is unimpeded for V626 and T630 in the closed state (Figure 5C), supporting the idea that no occlusion barrier for permeant ions exists between the extracellular solution and these positions. Finally, V626 and T630 do show state-dependent changes in the rate of modification for MTSEA, reacting about 210 and 510 times slower, respectively, in the absence rather than in the presence of glutamate. This relative difference, however, is small compared to that in voltage-dependent K^+ channels where positions with gated access have modification rates in the closed state up to 50,000 times slower than in the open state (Liu et al., 1997). Thus, the activation gate in NMDAR channels is located deep in the pore,

at the level of the N sites or deeper and presumably is associated with conformational changes in the M2 loop. As we argue below, the state-dependent decreases in reactivity we do see for extracellular vestibule positions, while not representing the activation gate, do represent key conformational changes coupling ligand binding to activation gate opening.

GluR channels and members of the voltage-gated family of ion channels (e.g., K^+ and cyclic nucleotide-gated [CNG]) share a similar, albeit inverted, architecture (Wo and Oswald, 1994; Chen et al., 1999). In K^+ channels, the activation gate is located at the intracellular end of the channel and is separated from the tip of the P loop by a large cavity (see Yellen, 1998). On the other hand, the activation gate in CNG channels is formed by the P loop (Sun et al., 1996; Liu and Siegelbaum, 2000), as presumably does the corresponding structure, the M2 loop, in NMDAR channels. Hence, CNG and NMDAR channels may share comparable gating mechanisms, at least in terms of the location of the activation gate. Alternatively, activation gating in the M2 loop could be mechanistically related to C-type inactivation in K^+ channels that also involves conformational changes in the P loop (Liu et al., 1996).

Constriction of the Extracellular Vestibule Pore Walls during Gating Underlies Trapping Block

Although positions within the extracellular vestibule do not form the activation gate, many of them showed a significant decrease in reactivity in the closed state (Figure 5). These slower rates could reflect that, upon channel closure, the electrostatic potential in the extracellular vestibule is reduced (e.g., Pascual and Karlin, 1998). However, positions with voltage-independent accessibility showed significant state-dependent changes in reactivity (F540, A635, L639, and N794), and, for positions with voltage-dependent access, some showed only small decreases in reactivity (N632 and L633), and they were intertwined between positions that showed much stronger decreases. Thus, the state-dependent changes in reactivity cannot be due solely to changes in the electrostatic potential following gate closure and must therefore reflect direct conformational changes concomitant with gating.

Positions deep in the pore, the N sites and V626 and T630 in M3, are protected by trapping blockers and the sequential blocker 9-AA (Figures 6 and 7). These deep positions therefore define the main blocking site for these compounds, a result supported by the strong voltage dependence of their action (Costa and Albuquerque, 1994; Blanpied et al., 1997; Sobolevsky et al., 1998). In the absence of glutamate, however, these same positions are accessible to externally applied Ag^+ and MTS reagents. Thus, the deep blocking site is external to the activation gate, indicating that in NMDAR channels trapping block does not arise via the blocker being trapped behind the activation gate. Consistent with this result is the finding that AM and MEM are imperfectly trapped, entering and leaving their deep blocking site via the same hydrophilic pathway both in the presence and absence of glutamate, though much slower in the latter case (Sobolevsky et al., 1998).

What is the mechanism underlying trapping block? One possibility is that the conformational changes in the extracellular vestibule alter the properties of the deep binding site, inducing it to have a much higher affinity for blockers in the closed than in the open state. However, given the diverse chemical nature of trapping blockers, such an increased affinity must arise via an electrostatic action, yet the reactivity of the positively charged MTSEA was reduced in the closed state for all deep positions (Figure 5). In addition, the same binding site would have to show the exact opposite affinity profile for the sequential blocker 9-AA, which keeps channels in the open state. An alternative explanation for trapping block is that with channel closure, the pore walls of the extracellular vestibule constrict. In this constricting model (Figures 8A and 8B), the narrowing of the water-filled pore in the extracellular vestibule is sufficient to trap moderately sized blockers (i.e., trapping blockers) but does not occlude ion fluxes with channel closure. This model would account for the consistent decrease in reactivity for exposed positions in the closed state (Figure 5) and explain how the larger-sized 9-AA, by occluding this constricting process, would prevent channel closure.

Where does constricting of the extracellular vestibule occur? At minimum, the pore walls constrict around the deep blocking site since V626 and T630 show the greatest relative decrease in reactivity in the closed state (Figure 5D), and 9-AA, which occupies this site, prevents channel closure (Figure 7B). Constricting may also occur more superficially, at least up to position A635 in the M3 segment where the absolute reactivity in the closed state was slowed to $<10^2$ $M^{-1}s^{-1}$ (Figure 5C). L544 in preM1, which also showed a voltage-dependent accessibility like the positions in M3, had a similar reduced absolute reactivity in the closed state. Consistent with the idea that the vestibule also constricts at more external locations is the finding that IEM-1857 and tetrapentylammonium (TPentA), which like 9-AA act as sequential blockers, occlude the pore at more superficial sites than 9-AA and trapping blockers (Antonov et al., 1998; Sobolevsky et al., 1999). Thus, a significant part of the pore walls in the extracellular vestibule—especially that contributed by the M3 segment—constrict in a concerted fashion during the process of channel closure, and restrictions placed on this movement in different parts of the pore prevent the entire process.

The sequential blocker 9-AA, occupying the deep blocking site near V626 and T630 in M3, prevents the extracellular vestibule from constricting. It also has two other significant actions; first, it increases the accessibility of L633 and A635 (Figure 7B), reflecting that 9-AA either expands the pore making access to these positions easier or increases NMDAR channel open probability. Second, 9-AA prevents the agonists glutamate and glycine from leaving their binding sites (Benveniste and Mayer, 1995). Thus, the multifaceted effects of 9-AA provide direct evidence for a causal relationship between agonist binding, gating-related movements of the M3 segment, and activation gate opening.

Structural and Functional Properties of the Extracellular Vestibule

The M3 segment contains the most highly conserved region, the SYTANLAAF motif, found in vertebrate GluRs (Beck et al., 1999). This motif also contains the Lurcher site, a position involved in controlling the gating properties

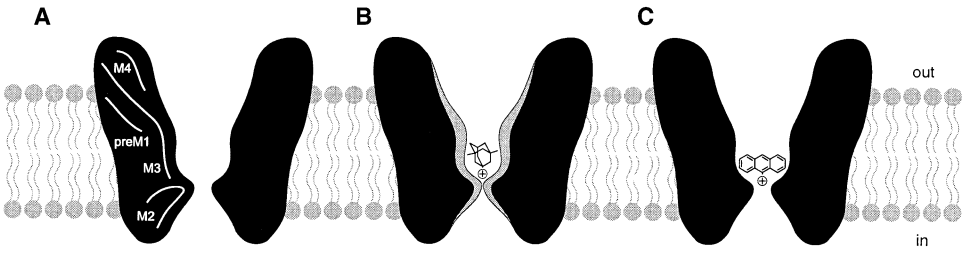

Figure 8. Model of NMDAR Channel during Gating and Block

(A) NMDAR channel in the open state. White lines on the black background of the channel protein indicate: (1) the M2 loop lining the intracellular vestibule with the tips of the loop forming the narrow constriction near the N site asparagines; (2) the M3 segment lining the deep part of the extracellular vestibule, where the voltage drop and binding of blockers occur; and (3) preM1, M4, and the region C-terminal to M3 forming the shallow part of the extracellular vestibule.

(B) The channel in the closed state with MEM trapped inside. Circled "+" indicates the charged amino group of the blocker. Gray regions symbolize those parts of the channel protein that move during channel gating, making the pore narrower with channel closure. In the closed state, these parts form the gate for permeant ions at the level of the N sites or deeper, and prevent trapped blockers from leaving the extracellular vestibule.

(C) The channel held in the open state by 9-AA. In the open state, 9-AA occupies the deep blocking site located close to the narrow constriction. In contrast to MEM (B), the large size of 9-AA prevents gating-related constricting in this region and, therefore, does not allow the activation gate to close.

of GluRs (Kohda et al., 2000) and determinants of Ca^{2+} influx in NMDAR channels, though the latter are mainly determined by regions C-terminal to M3 (J. Watanabe et al., submitted). Our results—by showing that the M3 segment forms the deep core of the extracellular vestibule including binding sites for open channel blockers—further extend the structural and functional significance of M3 in GluR channels.

The more shallow part of the extracellular vestibule is formed by preM1, the M4 segment and regions located C-terminal to M3 (Figure 8A). The finding that preM1 is located extracellularly suggests that the M1 segment itself is a membrane-spanning domain, buried in the protein and possibly in contact with the lipid bilayer. Much of the M4 segment, except for the very N-terminal part, presumably has a similar arrangement.

The common blocking site for trapping blockers and 9-AA and their different effects on channel gating provide insights into the size of the extracellular vestibule in the vicinity of the deep blocking site. At negative membrane potentials, the single positive charge the blockers possess will be preferentially oriented toward the intracellular vestibule. In the blocked state then, the critical dimension of these molecules is that perpendicular to the axis of symmetry going through the charged moiety, with MEM, the larger of the two trapping blockers, and 9-AA having perpendicular dimensions of approximately 8 Å and 11–12 Å, respectively (Figures 8B and 8C). Therefore, the diameter of the deep blocking site in the open state should be at least 11–12 Å to accommodate 9-AA. In the closed state, this same region should be smaller than this dimension but larger than 8 Å (the size of MEM and the head group of PTrEA). The channel's narrow constriction, having a diameter of approximately 5–6 Å and formed at the tip of the M2 loop (Wollmuth et al., 1996; Kuner et al., 1996), apparently lies adjacent to V626 in M3.

The M3 segment is a link coupling ligand binding to activation gate opening, presumably in the M2 loop. How the movement in M3 induces conformational changes in the M2 loop is unknown, but they could arise indirectly via the M2-M3 linker. Alternatively, the constricting of the pore walls as contributed by M3 could directly lead to a constricting of the M2 loops. Occlusion of ion fluxes would therefore occur at the tip of the M2 loops because of the smaller diameter of the pore formed by this region (that is, the channel's narrow constriction) in the open state.

Experimental Procedures

Heterologous Expression

All experiments were performed with previously described expression constructs for wild-type and mutant NMDAR subunits (Kuner et al., 1996; Beck et al., 1999). NR1 mutants were coexpressed with wild-type NR2C or vice versa in *Xenopus laevis* oocytes. Oocytes were prepared as described (Wollmuth et al., 1996) and were maintained in a nutrient OR-3 medium, containing 50% L-15, 50 μg/ml penicillin-streptomycin, 5 mM glutamine, and 15 mM Na-HEPES (pH 7.2, NaOH) (all GIBCO-BRL, Grand Island, NY). cRNA was transcribed and capped for each expression construct using SP6 RNA polymerase (Ambion Inc., Austin, TX) and examined electrophoretically on a denaturating agarose gel. RNA concentrations were determined by ethidium bromide stain of the gel relative to an RNA molecular weight marker. Dilutions of RNA (0.01–0.1 μg/μl) were prepared in order to achieve optimal expression. Oocytes were injected with 50 nl of RNA solution using a Nanoject II injector (Drummond Corp., Broomall, PA). Recordings were made 2–5 days after injections.

Current Recordings and Data Analysis

Whole-cell currents of *Xenopus* oocytes were recorded at room temperature (20°C–23°C) using two-electrode voltage clamp (DAGAN TEVA-200A, DAGAN Corp., Minneapolis, MN) with PULSE software (WaveMetrics Inc., Lake Oswego, OR). Microelectrodes were filled with 3 mM KCl and had resistances of 1–4 MΩ. To minimize solution exchange rates, we used a narrow flow-through recording chamber with a small volume of ~70 μl.

The external solution consisted of 115 mM NaCl, 2.5 mM KCl, 0.18 mM $CaCl_2$, and 10 mM HEPES (pH 7.2, NaOH). When Ag^+ was the test reagent, the solution was the same except that NO_3^- salts were used. All agonists, reagents, and blockers were applied with the bath solution. The concentration of glutamate and glycine was 200 μM and 10 μM, respectively. Glycine was added to all solutions except for those containing DL-2-amino-5-phosphonovaleric acid (APV).

Curve fitting was done using Igor Pro (WaveMetrics, Inc.) and Microcal Origin 4.1 (Northampton, MA). Results are presented as mean ± SEM. An ANOVA or a Student's t test was used to test for statistical differences. The Tukey test was used for multiple comparisons. Significance was assumed if $p < 0.05$.

Chemical Modification

NMDAR cysteine-substituted mutant channels were probed from the extracellular side of the membrane with methanethiosulfonate (MTS) reagents or Ag^+. The MTS reagents included the positively charged 2-aminoethyl MTS (MTSEA), 2-(trimethylammonium)ethyl MTS (MTSET), and 3-(triethylammonium)propyl MTS (PTrEA), and the neutral methyl MTS (MMTS). Stock solutions (2–100 mM) were made as aliquots (50–200 μl) under ice-cold conditions and were then frozen. Immediately before the experiment, an aliquot was thawed and diluted out to the concentration indicated in the text. With 2 mM or higher concentrations, the powder of the MTS reagent was dissolved immediately before application. Ag^+ solutions, always made and used in darkness, were prepared fresh daily from the powder. MTS reagents were purchased from Toronto Research Chemicals, Inc. (Ontario, Canada). All other chemicals were obtained from Sigma (St. Louis, MO).

Steady-State Reactions

Steady-state reactions were quantified at −60 mV. Baseline current amplitudes (I_{pre}) were established by five consecutive 15 s applications of glutamate separated by 90 to 120 s washes in glutamate-free solution. After the fifth application, PTrEA (2 mM) was applied for 60 s in the continuous presence of glutamate. After PTrEA, current amplitudes (I_{post}) were determined again using five glutamate applications. The change in the current amplitude, expressed as a percentage, was calculated as: $= (1 - I_{post}/I_{pre}) \times 100$. A comparable protocol was used to determine accessibility in the closed state except that PTrEA was applied in the absence of glutamate and APV was added to the extracellular solution 15 s before and removed 15 s after PTrEA exposure. The washout interval between the end of the PTrEA application and the first test glutamate application ranged from 1.25 to 5 min.

Reaction Rates

Reaction rates, measured at −60 mV except for Figure 3, were determined either by measuring the rate of change in current amplitudes during a continuous application of a sulfhydryl reagent ("continuous" protocol) (e.g., Figure 2A), or by applying a reagent for a specified amount of time and measuring current amplitudes before and after this application ("pulsive" protocol) (e.g., Figure 5A). For both protocols, changes in current amplitudes were fitted with a single exponential:

$$I = I_\infty + (I_0 - I_\infty) \exp(-t/\tau), \quad (1)$$

where t is the cumulative time of exposure to the reagent, I is the current after t seconds of this exposure, I_0 is the initial current (at $t = 0$), I_∞ is the asymptotic current when the reaction is complete, and τ is the time constant. The apparent second-order rate constant for chemical modification, k, was related to τ by:

$$k = 1/(\tau\,[C]), \quad (2)$$

where [C] is the concentration of Ag^+ or the MTS reagent.

Accurate measurements of reaction rates require that the rate of solution exchange be faster than the rate of the reaction itself. We adjusted the time of complete solution exchange, estimated from the kinetics of open tip responses, to <2 s for the "continuous" protocol and to ~10 s for "pulsive" protocols. MTS concentrations were selected such that τ was on the order of 10–40 s for the continuous protocol and 50–200 s for pulsive protocols. Current "run-down" during pulsive protocols was tested without applying sulfhydryl reagents for all mutant channels and was always less than 10%.

The voltage dependence of k was analyzed according to the following equation:

$$k = k_0 \exp(-z\delta F V_h/RT), \quad (3)$$

where V_h is the holding potential, k_0 is the apparent second-order rate constant for modification at $V_h = 0$, and $z\delta$ is the fraction of the transmembrane electric field the MTS reagent passes to reach the exposed cysteine. *F, R,* and *T* have their usual meaning. To derive $z\delta$, we rearranged Equation 3:

$$-(RT/F)\,\mathrm{Ln}\,k = A + z\delta V_h, \quad (4)$$

where A is $-(RT/F)\mathrm{Ln}k_0$, and fitted Equation 4 to plots of $-(RT/F)\mathrm{Ln}k$ against V_h.

Acknowledgments

We thank Drs T. Kuner, P. Brehm, and C. Jatzke for their comments on the manuscript, Drs P. Brehm and A. Shcherbatko for help in work with *Xenopus laevis*, and L. Rooney, S. Metz, and J. Grewal for technical assistance. This work was supported by NIH RO1 grant NS39102, including a Parkinson's Disease Supplement, and a Sinsheimer Scholars Award (L.P.W).

Received June 13, 2001; revised October 19, 2001.

References

Antonov, S.M., Gmiro, V.E., and Johnson, J.W. (1998). Binding sites for permeant ions in the channel of NMDA receptors and their effects on channel block. Nat. Neurosci. *1*, 451–456.

Armstrong, N., Sun, Y., Chen, G.-Q., and Gouaux, E. (1998). Structure of a glutamate-receptor ligand-binding core in complex with kainate. Nature *395*, 913–917.

Beck, C., Wollmuth, L.P., Seeburg, P.H., Sakmann, B., and Kuner, T. (1999). NMDAR channel segments forming the extracellular vestibule inferred from the accessibility of substituted cysteines. Neuron *22*, 559–570.

Benveniste, M., and Mayer, M.L. (1995). Trapping of glutamate and glycine during open channel block of rat hippocampal neuron NMDA receptors by 9-aminoacridine. J. Physiol. *483*, 367–384.

Blanpied, T.A., Boeckman, F., Aizenman, E., and Johnson, J.W. (1997). Trapping channel block of NMDA-activated responses by amantadine and memantine. J. Neurophysiol. *77*, 309–323.

Chen, H.-S.V., and Lipton, S.A. (1997). Mechanism of memantine block of NMDA-activated channels in rat retinal ganglion cells: uncompetitive antagonism. J. Physiol. *499*, 27–46.

Chen, G.-Q., Cui, C., Mayer, M.L., and Gouaux, E. (1999). Functional characterization of a potassium-selective prokaryotic glutamate receptor. Nature *402*, 817–821.

Costa, A.C.S., and Albuquerque, E.X. (1994). Dynamics of the actions of tetrahydro-9-aminoacridine and 9-aminoacridine on glutamatergic currents: concentration-jump studies in cultured rat hippocampal neurons. J. Pharmacol. Exp. Ther. *268*, 503–514.

Dingledine, R., Borges, K., Bowie, D., and Traynelis, S.F. (1999). The glutamate receptor ion channels. Pharmacol. Rev. *51*, 7–61.

Huettner, J.E., and Bean, B.P. (1988). Block of NMDA-activated current by the anticonvulsant MK-801: selective binding to open channels. Proc. Natl. Acad. Sci. USA *85*, 1307–1311.

Karlin, A., and Akabas, M.H. (1998). Substituted-cysteine accessibility method. Methods Enzymol. *293*, 123–145.

Kohda, K., Wang, Y., and Yuzaki, M. (2000). Mutation of a glutamate receptor motif reveals its role in gating and δ2 receptor properties. Nat. Neurosci. *3*, 315–322.

Krupp, J.J., Vissel, B., Heinemann, S.F., and Westbrook, G.L. (1996). Calcium-dependent inactivation of recombinant N-methyl-d-aspartate receptors is NR2 subunit specific. Mol. Pharmacol. *50*, 1680–1688.

Krupp, J.J., Vissel, B., Heinemann, S.F., and Westbrook, G.L. (1998). N-terminal domains in the NR2 subunit control desensitization of NMDA receptors. Neuron *20*, 317–327.

Kuner, T., Wollmuth, L.P., Karlin, A., Seeburg, P.H., and Sakmann, B. (1996). Structure of the NMDA receptor channel M2 segment inferred from the accessibility of substituted cysteines. Neuron *17*, 343–352.

Liu, J., and Siegelbaum, S.A. (2000). Change of pore helix conformational state upon opening of cyclic nucleotide-gated channels. Neuron *28*, 899–909.

Liu, Y., Jurman, M.E., and Yellen, G. (1996). Dynamic rearrangement of the outer mouth of a K^+ channel during gating. Neuron *16*, 859–867.

Liu, Y., Holmgren, M., Jurman, M.E., and Yellen, G. (1997). Gated access to the pore of a voltage-dependent K^+ channel. Neuron *19*, 175–184.

MacDonald, J.F., Bartlett, M.C., Mody, I., Pahapill, P., Reynolds, J.N., Salter, M.W., Schneiderman, J.H., and Pennefather, P.S. (1991). Actions of ketamine, phencyclidine and MK-801 on NMDA receptor currents in cultured mouse hippocampal neurons. J. Physiol. *432*, 483–508.

Parsons, C.G., Danysz, W., and Quack, G. (1998). Glutamate in CNS disorders as a target for drug development: an update. Drug News Perspect. *11*, 523–569.

Pascual, J.M., and Karlin, A. (1998). State-dependent accessibility and electrostatic potential in the channel of the acetylcholine receptor. Inferences from rates of reaction of thiosulfonates with substituted cysteines in the M2 segment of the α subunit. J. Gen. Physiol. *111*, 717–739.

Sobolevsky, A.I. (1999). Two-component blocking kinetics of open NMDA channels by organic cations. Biochim. Biophys. Acta *1416*, 69–91.

Sobolevsky, A., and Koshelev, S. (1998). Two blocking sites of amino-adamantane derivatives in open N-methyl-D-aspartate channels. Biophys. J. *74*, 1305–1319.

Sobolevsky, A.I., and Yelshansky, M.V. (2000). The trapping block of NMDA-receptor channels in acutely isolated rat hippocampal neurones. J. Physiol. *526*, 493–506.

Sobolevsky, A.I., Koshelev, S.G., and Khodorov, B.I. (1998). Interaction of memantine and amantadine with agonist-unbound NMDA-receptor channels in acutely isolated rat hippocampal neurons. J. Physiol. *512*, 47–60.

Sobolevsky, A.I., Koshelev, S.G., and Khodorov, B.I. (1999). Probing of NMDA channels with fast blockers. J. Neurosci. *19*, 10611–10626.

Sun, Z.-P., Akabas, M.H., Goulding, E.H., Karlin, A., and Siegelbaum, S.A. (1996). Exposure of residues in the cyclic nucleotide-gated channel pore: P region structure and function in gating. Neuron *16*, 141–149.

Villarroel, A., Regalado, M.P., and Lerma, J. (1998). Glycine-independent NMDA receptor desensitization: localization of structural determinants. Neuron *20*, 329–339.

Wo, Z.G., and Oswald, R.E. (1994). Transmembrane topology of two kainite receptor subunits revealed by N-glycosylation. Proc. Natl. Acad. Sci. USA *91*, 7154–7158.

Wollmuth, L.P., Kuner, T., Seeburg, P.H., and Sakmann, B. (1996). Differential contribution of the NR1- and NR2A-subunits to the selectivity filter of recombinant NMDA receptor channels. J. Physiol. *491*, 779–797.

Yeh, J.Z., and Armstrong, C.M. (1978). Immobilisation of gating charge by a substance that simulates inactivation. Nature *273*, 387–389.

Yellen, G. (1998). The moving parts of voltage-gated ion channels. Q. Rev. Biophys. *31*, 239–295.